

GeoVLA: Empowering 3D Representations in Vision-Language-Action Models

Lin Sun^{1*†} Bin Xie^{2†} Yingfei Liu² Hao Shi³ Tiancai Wang² Jiale Cao^{1‡}

¹Tianjin University ²Dexmal ³Tsinghua University

{sun0806,connor}@tju.edu.cn, {xiebin,lyf,wtc}@dexmal.com

Abstract

Vision-Language-Action (VLA) models have emerged as a promising approach for enabling robots to follow language instructions and predict corresponding actions. However, current VLA models mainly rely on 2D visual inputs, neglecting the rich geometric information in the 3D physical world, which limits their spatial awareness and adaptability. In this paper, we present GeoVLA, a novel VLA framework that effectively integrates 3D information to advance robotic manipulation. It uses a vision-language model (VLM) to process images and language instructions, extracting fused vision-language embeddings. In parallel, it converts depth maps into point clouds and employs a customized point encoder, called Point Embedding Network, to generate 3D geometric embeddings independently. These produced embeddings are then concatenated and processed by our proposed spatial-aware action expert, called 3D-enhanced Action Expert, which combines information from different sensor modalities to produce precise action sequences. Through extensive experiments in both simulation and real-world environments, GeoVLA demonstrates superior performance and robustness. It achieves state-of-the-art results in the LIBERO and ManiSkill2 simulation benchmarks, and shows remarkable robustness in real-world tasks requiring height adaptability, scale awareness and viewpoint invariance. The project is available at <https://linsun449.github.io/GeoVLA>.

1 Introduction

Advancing robot manipulation requires both intellectual interaction and precise physical motion control in real world. Recently, vision-language-action (VLA) models, capable of instruction following and robotic action execution, have attracted significant attention. To leverage general knowledge, most VLA models are built upon vision-language models (VLMs) (Liu et al., 2023b; Alayrac et al., 2022; Chen et al., 2023; Karamcheti et al., 2024; Bai et al., 2023) and develop through specialized designs for action generation. Early approaches such as RT-2 (Brohan et al., 2023a) and OpenVLA (Kim et al., 2025b) quantize the action space into discrete bins and adopt autoregressive token generation. While compatible with standard VLM architectures, this coarse representation struggles with complex, fine-grained manipulation tasks. To address this issue, some approaches (Bjorck et al., 2025; Black et al., 2025; Li et al., 2024; Liu et al., 2025a) introduce specialized action experts that process features from VLMs and output action chunking (Zhao et al., 2023) with diffusion processes (Ho et al., 2020) or flow matching (Lipman et al., 2022) to directly parameterize continuous action spaces.

Despite these advancements, current VLA models predominantly rely on 2D visual inputs, overlooking the rich geometric priors inherent in 3D physical world. In contrast, 3D geometric information inherently provides accurate depth cues, enhanced spatial understanding, and robustness to viewpoint

*This work was done during the internship at Dexmal.

†Equal contribution.

‡Corresponding author: Jiale Cao

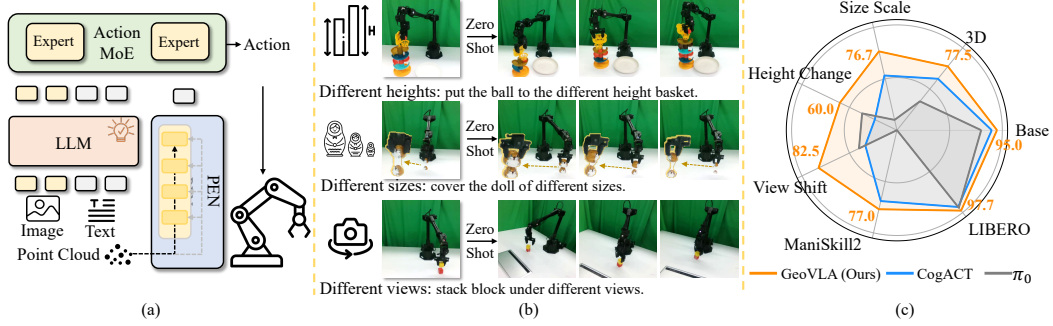


Figure 1: GeoVLA adopts two parallel architecture shown in (a), which additionally extracts 3D geometric information from the point cloud to guide action generation. In this way, GeoVLA shows robust adaptability to height, size, and view variations in (b), and outperforms other methods in (c).

changes. Building on recent advances in 3D perception, emerging approaches such as LLaVA-3D (Zhu et al., 2024) and SpatialVLA (Qu et al., 2025) integrate 3D positional encodings into VLMs to enable geometrically-aware representations. However, this integration disrupts the alignment between visual encoders and Large Language Models (LLMs). Consequently, bridging this misalignment often requires large-scale 3D embodied instruction-tuning datasets. As an alternative to such data-intensive approaches, another line of work focuses on injecting 3D information directly into action experts. For instance, PointVLA (Li et al., 2025) adopts a two-stage training scheme: it first trains a 2D-VLA model, then freezes the action expert and injects point cloud features through a zero-initialized ControlNet-style module (Zhang et al., 2023). However, although freezing the action expert preserves its low-level capabilities, it hinders adaptation to the newly introduced point cloud modality. Therefore, integrating 3D information into VLA frameworks in an end-to-end manner remains a key challenge.

In this paper, we present GeoVLA, a novel VLA framework that integrates 3D information in an elegant way. As shown in Fig. 1(a), GeoVLA incorporates a customized point encoder, Point Embedding Network (PEN), and a spatial-aware action expert, 3D-enhanced Action Expert (3DAE), to bridge the gap between 2D and 3D modalities. Specifically, GeoVLA employs a VLM to process images and language instructions, extracting fused vision-language embeddings. Concurrently, it transforms the depth map into a point cloud and utilizes the PEN to independently generate 3D geometric embeddings. This dual-path design preserves the pre-trained knowledge and general understanding capabilities of the VLM. Subsequently, these embeddings are concatenated and processed by our novel 3DAE module. The 3DAE employs two specialized experts to jointly model information from both visual and point cloud modalities, ultimately generating precise action sequences. In this way, our GeoVLA achieves the multi-modal alignment and superior performance.

We evaluate GeoVLA through both simulation and real-world experiments. In LIBERO (Liu et al., 2023a), our GeoVLA outperforms previous SoTA method OpenVLA-OFT (Kim et al., 2025a) by 2.4%. For ManiSkill2 (Mu et al., 2021), it outperforms Dita (Hou et al., 2025) by 11%. In real-world experiments, GeoVLA achieves an average success rate of 86.3% in 8 tasks, outperforming π_0 (Black et al., 2025) by 28.8%. Furthermore, GeoVLA exhibits superior robustness in scenarios requiring height adaptation, scale awareness and viewpoint generalization as shown in Fig. 1(b).

In summary, our contributions are as follows:

- We propose GeoVLA, a novel Vision-Language-Action (VLA) framework that incorporates both visual and point cloud modalities. Unlike prior work focusing solely on 2D features, GeoVLA explicitly processes multi-modal inputs through parallel branches. This design equips the model with stronger spatial understanding and geometric awareness, maintaining generalization capabilities on height adaptability, scale awareness and viewpoint invariance.
- We introduce the Point Embedding Network (PEN) and 3D-enhanced Action Expert (3DAE). PEN extracts discriminative geometry-aware features, while the 3DAE module leverages modality-specific experts to integrate visual and geometric cues effectively.
- Our proposed GeoVLA achieves state-of-the-art performance on the LIBERO and ManiSkill2 benchmarks. It demonstrates significant advantages in incorporating 3D perception, exhibiting robustness in real-world robotic tasks, as shown in Fig. 1(c).

2 Related Works

Vision Language Action (VLA) Models: VLA aims to translate natural language instructions and visual observations into executable robot actions, typically building on pretrained vision-language models (VLMs). Early approaches such as RT-1 (Brohan et al., 2023b) and RT-2 (Brohan et al., 2023a) adopt a language-modeling perspective, discretizing actions into tokens and employing autoregressive decoders for token generation. OpenVLA (Kim et al., 2025b) extends this paradigm by introducing a large-scale multi-task instruction-following corpus. Recent works such as π_0 (Black et al., 2025) Rdt-1b (Liu et al., 2025b) and CogACT (Li et al., 2024) improve the model by generating continuous actions through flow matching (Lipman et al., 2022) or diffusion (Ho et al., 2020). By decoupling action representation from tokenization, they achieve more accurate modeling of motion trajectories. However, most VLA models rely solely on 2D RGB inputs, limiting their capacity to reason about spatial structure and depth, which are crucial in real-world scenarios.

3D Perception in VLA Models: With the advancement of 3D foundation models (Wang et al., 2024; Zhu et al., 2024; Zheng et al., 2025; Zhang et al., 2025), recent studies (Shridhar et al., 2023; Jia et al., 2024; Goyal et al., 2024; Ze et al., 2024) have explored various 3D representations to enhance robotic manipulation. Meanwhile, the emergence of VLA models, which leverage the pretraining power of VLMs, has opened new directions for generalizable policy learning. But how to integrate 3D perception into VLA models is still a growing research focus, driven by the limitations of purely 2D inputs in physical environments. Several works (Zhen et al., 2024b; Qu et al., 2025; Bhat et al., 2025; Li et al., 2025) aim to make VLA models geometry-aware by introducing 3D features such as depth maps, point clouds, or spatial position embeddings. For example, 3D-VLA (Zhen et al., 2024a) and 3D-CAVLA (Bhat et al., 2025) directly encode the 3D features as the embeddings to the VLM. While SpatialVLA (Qu et al., 2025) introduces spatial position embeddings derived from point clouds to equip the visual embeddings. These methods improve spatial reasoning capabilities, but often disrupt the alignment between vision representations and VLMs. Recovering this alignment typically demands additional embodied instruction tuning stages, which can be costly or laborious. For instance, ACT (Dong et al., 2023) mitigates the need for extensive task-specific fine-tuning on diverse multitask data to strong cross-task generalization. Similarly, LLARVA (Niu et al., 2024) highlights the difficulty of incorporating voxel or point cloud representations into existing vision-language structures and resorts to abstract 2D visual traces to maintain compatibility. These adaptations underscore the trade-off between injecting spatial knowledge and preserving pretrained alignment during deployment.

Modality-Aware Action Experts and Point Cloud Fusion: To preserve the alignment of VLA models while incorporating 3D information, a complementary line of work explores injecting geometry into action heads rather than modifying visual backbones. PointVLA (Li et al., 2025) introduces a zero-initialized 3D feature injector that injects point cloud features into export policy. This design avoids the need to retrain action experts. However, it hinders adaptation to the newly introduced point cloud modality.

Our proposed method, GeoVLA, distinguishes itself by employing a specialized point encoder (Point Embedding Network) to process 3D inputs independently, and a spatial-aware action expert (3D-enhanced Action Expert) that explicitly models the interaction between visual-language and point cloud representations through modality-specific experts. This design preserves pretrained knowledge, enables more expressive 3D fusion, and improves performance in both simulation benchmarks and real-world robotic tasks.

3 Methodology

3.1 Problem Definition

In the general formulation of vision-language-action (VLA) models, the input consists of two modalities: a visual observation and a natural language instruction. The output is a sequence of actions. Specifically, the visual observation V is typically an RGB image captured from a fixed or egocentric camera, while the language instruction L describes the task to be performed. Given V and L , the policy p , represented by a pre-trained VLA model, generates a sequence of actions $a_{1:T}$, where T is a hyperparameter that defines the size of the action chunk. Formally,

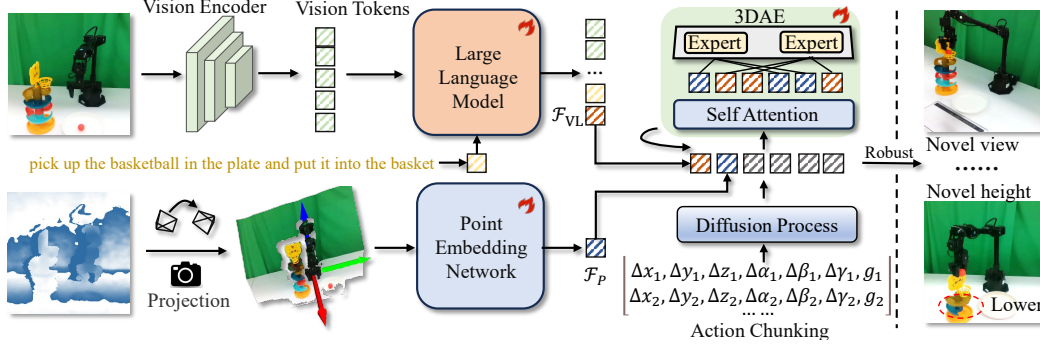


Figure 2: **Overview of GeoVLA.** RGB images with language instructions are processed by a VLM to produce vision–language features \mathcal{F}_{VL} , while depth maps are reprojected into point clouds and encoded by PEN as geometric features \mathcal{F}_P . Both modalities are combined in 3DAE to progressively generate robot actions.

$$a_{1:T} \sim p(a_{1:T} \mid V, L) \quad (1)$$

Each action a_t in the sequence, where $1 \leq t \leq T$, represents a relative movement from the current state of robot, and is typically parameterized as follows:

$$a_t = (\Delta x, \Delta y, \Delta z, \Delta \alpha, \Delta \beta, \Delta \gamma, g) \quad (2)$$

Here, $(\Delta x, \Delta y, \Delta z)$ denotes the relative translation, $(\Delta \alpha, \Delta \beta, \Delta \gamma)$ denotes the relative rotation (*e.g.*, in Euler angles), and g is the absolute gripper command.

To enhance the spatial perception capabilities of VLA models, we incorporate an additional point cloud P , typically obtained from RGB-D camera. The policy then conditions on the visual input V , the point cloud P , and the language instruction L to generate the action sequence:

$$a_{1:T} \sim p(a_{1:T} \mid V, P, L) \quad (3)$$

3.2 Overview

As illustrated in Fig. 2, GeoVLA is an end-to-end VLA framework that processes visual and geometric information simultaneously. The pipeline comprises three key components: a VLM for general understanding of visual and language modalities, a Point Embedding Network (PEN) for extracting fine-grained 3D geometric features, and a 3D-enhanced Action Expert (3DAE) for generating action chunk sequences.

Specifically, given the image V and the language instruction L , GeoVLA leverages a pre-trained 2D VLM (*e.g.*, Prismatic (Karamcheti et al., 2024)) to extract a general understanding \mathcal{F}_{VL} of current environment. Concurrently, the depth map D is projected into a 3D point cloud P using the camera parameters. The point cloud is processed by the PEN, which is designed to extract a 3D feature \mathcal{F}_P centered on the end-effector, capturing critical structural and spatial cues. The extracted features \mathcal{F}_{VL} and \mathcal{F}_P are then concatenated and serve as conditional inputs to the 3DAE. Based on denoising diffusion principles, 3DAE starts from a noisy action sequence and progressively refines the noise, guided by the multi-modal context. The mixed expert architecture enables specialized processing of the heterogeneous features \mathcal{F}_{VL} and \mathcal{F}_P . Each expert learns to capture complementary aspects, thereby enhancing the capacity to generate context-aware and precise action sequences.

3.3 Point Embedding Network

Due to the inherent noise in the original depth map, extracting compact and clean geometric features is critically important. We propose Point Embedding Network (PEN), a novel geometric point encoder designed for robotic manipulation that captures fine-grained 3D structural cues centered at the end-effector.

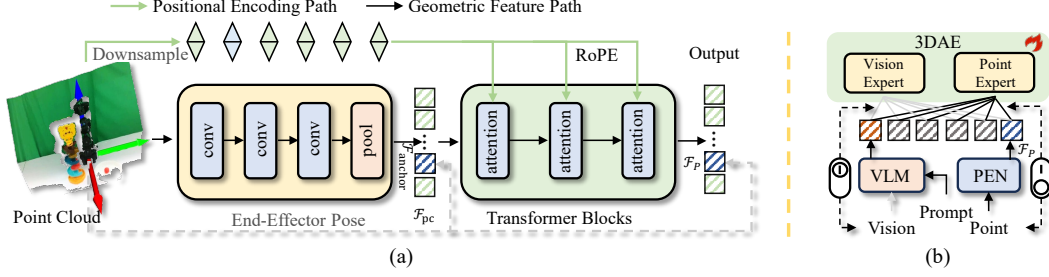


Figure 3: **Dual-path Point Embedding Network.** In (a) Point Embedding Network processes the point cloud through two parallel paths: geometric feature path using large-kernel convolutions, and a positional encoding path leveraging RoPE to preserve 3D spatial information. In (b) only the selected \mathcal{F}_P is send to the action expert along with visual feature.

As illustrated in Fig. 3(a), PEN first converts the raw depth map captured by an RGB-D camera (e.g., RealSense) into a point cloud P expressed in the end-effector coordinate system, where the current end-effector position of robot is at the origin. The encoder then adopts a dual-path architecture: (1) *Geometric feature path.* A lightweight CNN equipped with multi-layer large-kernel convolutions and local pooling encodes the point cloud into patch-level geometric tokens: $\mathcal{F}_{pc} \in \mathbb{R}^{N \times C}$, where N is the number of tokens and C is the feature dimension, followed by the transformer blocks to aggregate the useful global information. (2) *Positional encoding path.* The original point cloud is downsampled to match the size of \mathcal{F}_{pc} and guides the position information by rotary positional encoding (RoPE) (Su et al., 2024).

Subsequently, PEN selects the token corresponding to the coordinate origin (e.g., the end-effector token) as the anchor token \mathcal{F}_{anchor} (colored blue in Fig. 3(a)) and feeds the geometric tokens \mathcal{F}_{pc} into transformer blocks, where the tokens interact under the guidance of manually generated RoPE. Finally, we only select the updated anchor token from the last transformer layer as the encoded feature \mathcal{F}_P to guide the action export as shown in Fig. 3(b).

This spatial anchor design offers two key benefits: (1) *Focused representation learning.* The attention mechanism concentrates on manipulation-relevant regions, improving feature extraction efficiency. (2) *Explicit spatial relationship modeling.* Critical geometric relationships between the end-effector and surrounding objects are captured, enabling precise contact prediction. By delivering localized yet context-aware 3D structural features to downstream action policies, PEN facilitates spatially grounded decision-making with improved physical coherence.

3.4 3D-enhanced Action Expert

As illustrated in Fig. 2, the 3D-enhanced Action Expert (3DAE) employs the Diffusion Transformers (DiTs) (Peebles and Xie, 2023) architecture designed to process concatenated multi-modal tokens (\mathcal{F}_{VL} and \mathcal{F}_P) and generate action sequences. During training, the future action sequence $(\Delta x, \Delta y, \Delta z, \Delta \alpha, \Delta \beta, \Delta \gamma, g)$, sampled from recorded observations, is gradually perturbed to generate a noisy sequence by diffusion process. The noisy actions are served as action tokens and concatenated with the multi-modal tokens. The combined tokens are fed into the diffusion transformer for interaction, ultimately predicting the added noise. During inference, we first sample a noise distribution using DDIM (Song et al., 2021) and then, conditioned on multi-modal tokens, progressively recover the desired action sequence.

However, effectively integrating features from different modalities presents a significant challenge. To leverage the complementary strengths of vision-language features \mathcal{F}_{VL} and geometric features \mathcal{F}_P , we introduce a novel Mixture-of-Experts (MoE) architecture within the feed-forward networks (FFNs) of our diffusion transformer action head 3DAE. This design enables specialized processing for each modality, allowing the model to more effectively utilize multi-modal conditional information.

Since the VLM branch is pre-trained while the point cloud branch is initialized from scratch, our experimental results indicate that directly applying a dynamic routing mechanism inherently biases the model toward the VLM branch. To mitigate this imbalance, we introduce a static routing strategy. During training, we randomly drop one modality in each iteration, resulting in three distinct input configurations: (1) vision-language features only, (2) language and geometric features, where RGB

image tokens are removed before being fed into the VLM, and (3) the full multi-modal input. In 3DAE, the activation of each expert is deterministically governed by the presence and relevance of input modalities. This static, purpose-driven routing strategy within the MoE architecture ensures that the unique strengths of each modality are effectively leveraged. At the same time, it maintains the powerful generative capabilities of the DiT, enabling robust and comprehensive action chunk generation for robotic control.

4 Simulation Experiments

In this section, we conduct a thorough evaluation of GeoVLA on two widely-used robotic manipulation benchmarks, LIBERO (Liu et al., 2023a) and ManiSkill2 (Mu et al., 2021), to assess the effectiveness and scalability of our approach across diverse tasks.

LIBERO consists of five task suites, spanning four unique scenes. Each suite is designed to evaluate specific capabilities:

- **LIBERO-Spatial** focuses on placing the same object in different positions.
- **LIBERO-Object** involves placing different objects into a box within a fixed scene layout.
- **LIBERO-Goal** evaluates the ability to perform diverse operations in a fixed layout.
- **LIBERO-Long**, also called LIBERO-10, which targets 10 long-horizon tasks involving varied scenes and operations.
- **LIBERO-90** is an expanded version of LIBERO-10, presents a more challenging benchmark.

The more visualization of LIBERO benchmark can be found in Fig .5(a).

ManiSkill2 focuses more on basic pick-and-place capabilities. Following Dita (Hou et al., 2025), we evaluate our approach on five representative tasks: *PickCube*, *StackCube*, *PickSingleYCB*, *PickSingleEGAD*, and *PickClutterYCB*. Except for *StackCube*, each task requires the robot to grasp a specified object and place it at a designated 3D position indicated by a green marker, making them well-suited to evaluate 3D perception and spatial reasoning. Furthermore, *PickSingleYCB* and *PickSingleEGAD* introduce greater challenges by varying the objects, with a combined total of around 1700 distinct objects. *PickClutterYCB* is even more challenging, requiring the robot to identify and select the correct object from a cluttered scene containing up to 74 different types of YCB (Xiang et al., 2018) objects. The more visualizations of ManiSkill2 benchmark can be found in Fig .5(b).

4.1 Implementation Details

The VLM component in GeoVLA is Prismatic-7B (Karamcheti et al., 2024), initialized using the pre-trained weights released by OpenVLA (Kim et al., 2025b), which is trained on the large-scale Open X-Embodiment dataset (O’Neill et al., 2024). In contrast, both the proposed PEN and 3DAE are randomly initialized. All experiments are conducted on 8 NVIDIA A100 GPUs using the Fully Sharded Data Parallel (FSDP) strategy. Each GPU processes a batch size of 32, resulting in a total batch size of 256. Optimization is performed using the AdamW optimizer (Loshchilov and Hutter, 2019) with a constant learning rate of 2×10^{-5} . Mixed-precision training (Micikevicius et al., 2018) is enabled to improve efficiency and reduce memory consumption. The dataset is loaded via TensorFlow Datasets (TFDS), with a shuffle buffer size of 10,000. No data augmentation is applied during training. For action modeling, we adopt a chunking strategy with a fixed length of $T = 16$.

For the LIBERO benchmark (Liu et al., 2023a), GeoVLA processes only a single main camera view together with the point cloud map derived from the corresponding depth image, without incorporating any additional inputs (*e.g.*, pose states or wrist-view images). In contrast, for ManiSkill2 (Mu et al., 2021), additional information is provided, including the proprioceptive state, the gripper state, and the target marker position since there are some occlusions in the image. Training runs for both benchmarks approximately 20,000 steps (about 20 hours), corresponding to roughly 6 epochs on LIBERO and 2 epochs on ManiSkill2. During inference, we follow the standard evaluation protocol: each LIBERO task is assessed over 50 independent episodes, while each ManiSkill2 task is evaluated over 20 episodes. All results are reported in terms of success rate (SR).

Table 1: **Results on LIBERO.** * denotes methods that incorporate extra proprioceptive states or wrist-camera images. Results of CogACT are reproduced by us. For methods not evaluated on LIBERO-90, the average success rate across the first four suites is reported.

Method	Spatial	Object	Goal	Long	LIBERO-90	Avg.
Octo (Octo Model Team et al., 2024)	78.9	85.7	84.6	51.1	-	75.1
OpenVLA (Kim et al., 2025b)	84.7	88.4	79.2	53.7	73.5	75.9
SpatialVLA (Qu et al., 2025)	88.2	89.9	78.6	55.5	46.2	71.7
π_0 -FAST* (Pertsch et al., 2025)	96.4	96.8	88.6	60.2	83.1	85.0
π_0 * (Black et al., 2025)	96.8	98.8	95.8	85.2	-	94.2
CogACT (Li et al., 2024)	<u>97.2</u>	98.0	90.2	88.8	<u>92.1</u>	93.2
OpenVLA-OFT* (Kim et al., 2025a)	96.2	98.3	<u>96.2</u>	<u>90.7</u>	-	<u>95.3</u>
GeoVLA (Ours)	98.4	99.0	96.6	96.6	97.7	97.7

Table 2: **Results on ManiSkill2.** * denotes our reproduced results. All the results are reported in terms of success rate (%).

Method	PickCube	StackCube	PickSingleYCB	PickSingleEGAD	PickClutterYCB	Avg.
OpenVLA* (Kim et al., 2025b)	65	55	0	15	0	27
Dita (Hou et al., 2025)	79	80	62	72	<u>36</u>	66
CogACT* (Li et al., 2024)	95	<u>90</u>	<u>65</u>	<u>75</u>	25	<u>69</u>
GeoVLA (Ours)	<u>90</u>	90	75	85	45	77

4.2 Main Results

LIBERO. Tab. 1 compares GeoVLA with several strong baselines on the LIBERO (Liu et al., 2023a) benchmark. GeoVLA delivers the best performance across all tasks. In particular, for the LIBERO-Long and LIBERO-90 tasks, GeoVLA achieves success rates of 96.6% and 97.7%, improving by 5.9% and 5.6%, respectively. Overall, GeoVLA achieves an average success rate of 97.7%, outperforming both CogACT (Li et al., 2024) (93.2%) and OpenVLA-OFT (Kim et al., 2025a) (95.3%).

ManiSkill2. Tab. 2 presents our results on the ManiSkill2 (Mu et al., 2021) benchmark. GeoVLA achieves the highest overall success rate of 77%, clearly surpassing both CogACT (69%) and Dita (66%). Specifically, on basic tasks such as *PickCube*, GeoVLA performs on par with CogACT, the best-performing method. However, on more challenging tasks like *PickClutterYCB*, GeoVLA achieves the best performance, with a success rate of 45% compared to 36% for Dita. Other methods struggle to improve their performance as the diversity of objects significantly increases the difficulty of 6D pose estimation. This challenge arises from the increased complexity of spatial position estimation due to object diversity. In contrast, GeoVLA leverages point cloud observations to maintain precise spatial awareness, resulting in substantially higher success rates on these more difficult tasks.

4.3 Ablation Study

To assess the impact of key components in our proposed GeoVLA, we perform a comprehensive ablation study on the LIBERO benchmark, the results of which are summarized in Tab. 3.

Comparison with Other Point Cloud Encoders. The effect of different point cloud encoders is examined by comparing a 3-layer MLP (e.g., DP3 (Ze et al., 2024)), PointNet (Qi et al., 2017), and the proposed PEN encoder. Tab. 3(a) illustrates that the MLP and PointNet encoders achieve success rates of 95.8% and 95.2%, respectively, while the PEN encoder outperforms them with a success rate of 97.7%, demonstrating its superior ability to capture geometric structure.

Different Anchor Token Selection Strategies. Three anchor token selection strategies are evaluated in Fig. 3(b): max pooling (*Max*), average pooling (*Mean*), and directly using the end-effector token (*End Effector*) as the pooled representation. The *End Effector* strategy achieves the best results (97.7%) compared to the *Max* (96.3%) and *Mean* (95.9%), suggesting that the end-effector token carries more task-relevant and informative features.

Impact of Position Embeddings. The role of Rotary Positional Embedding (*RoPE*) in the PEN encoder is examined in Fig. 3(c). Compared to the original 1D learnable position embeddings, incorporating *RoPE* consistently improves performance, increasing the success rate from 95.4% to 97.7%, confirming its effectiveness in enhancing spatial encoding.

Table 3: **Ablation Study.** For PEN, the ablation study demonstrates its efficiency by (a) comparing with other point encoders, (b) the anchor token selection strategy, and (c) analyzing the impact of position embeddings. For 3DAE, the effectiveness of the MoE-based design is evaluated.

Method		Spatial	Object	Goal	Long	LIBERO-90	Avg.
(a)	MLP	97.6	99.0	97.8	88.4	96.1	95.8
	PointNet	94.8	96.2	95.4	94.8	95.0	95.2
	PEN	98.4	99.0	96.6	96.6	97.7	97.7
(b)	Max	98.2	98.2	95.4	94.6	95.0	96.3
	Mean	98.0	96.6	95.2	92.6	97.2	95.9
	End Effector	98.4	99.0	96.6	96.6	97.7	97.7
(c)	1D PE	95.2	98.2	96.4	92.0	95.2	95.4
	RoPE	98.4	99.0	96.6	96.6	97.7	97.7
(d)	None MoE	98.0	98.4	94.6	93.2	95.7	96.0
	Dynamic Routing	98.4	98.4	98.4	94.8	96.6	97.3
	Static Routing	98.4	99.0	96.6	96.6	97.7	97.7

Table 4: **Success rate (%) on in-domain tasks.** GeoVLA achieves better performance compared with OpenVLA, π_0 , and CogACT.

Method	P-Carrot	S-Block	S-Cup	I-Circle	H-Cup	P-Basketball	C-Matryoshka	P-Hairclip	Avg.
OpenVLA (Kim et al., 2025b)	50	10	40	30	0	20	10	0	20.0
π_0 (Black et al., 2025)	100	50	90	80	50	40	50	0	57.5
CogACT (Li et al., 2024)	100	80	100	80	50	60	70	70	76.3
GeoVLA (Ours)	100	80	100	100	70	90	70	80	86.3

The Effectiveness of MoE Design in 3DAE. Fig. 3(d) compares the performance of our MoE-based 3DAE with non-MoE action heads commonly used in VLA models. Our MoE-based design achieves a performance gain of 96.0% to 97.7%. Although dynamic routing is the default in most MoE architectures, our experiments show that static routing performs better, likely due to its reduced bias towards the vision-language modalities during training.

5 Real-world Experiments

In this section, we validate GeoVLA through real-world robotic experiments involving various 3D manipulation tasks. These experiments demonstrate the robustness and generalization of GeoVLA, particularly under common deployment variations of the camera viewpoint, height, and object size.

Environment Setup. In our real-world experiments, we employ a WidowX-250s robotic arm with six degrees of freedom and a RealSense-435i depth camera placed approximately 0.8 meters away to capture a third-person viewpoint as shown in Fig. 8. The training setup mirrors the simulation experiments, with the training duration shortened to about 8 hours due to the smaller dataset. Each task is evaluated over 10 independent trials during inference.

5.1 Task Definition

A diverse set of tasks is used to evaluate GeoVLA, as shown in Fig. 9 of the supplementary material. These tasks include basic manipulation tasks such as *Pick Carrot* (P-Carrot), *Stack Block* (S-Block), *Stack Cup* (S-Cup), and *Insert Circle* (I-Circle), as well as 3D-aware tasks like *Hang Cup* (H-Cup), *Put Basketball* (P-Basketball), *Cover Matryoshka* (C-Matryoshka), and *Put Hairclip* (P-Hairclip), which test spatial perception and precise manipulation. We also introduce challenging task variations to assess spatial robustness during inference: (1) Varying the basket height in *Put Basketball* to test adaptability to target position changes. (2) Changing the camera viewpoint in *Stack Block* to evaluate viewpoint invariance. (3) Scaling the doll size in *Cover Matryoshka* to assess relative size perception. (4) Removing the sponge mat in *Pick Carrot* to test robustness to height variations in carrot placement. More details are available in the supplementary material.

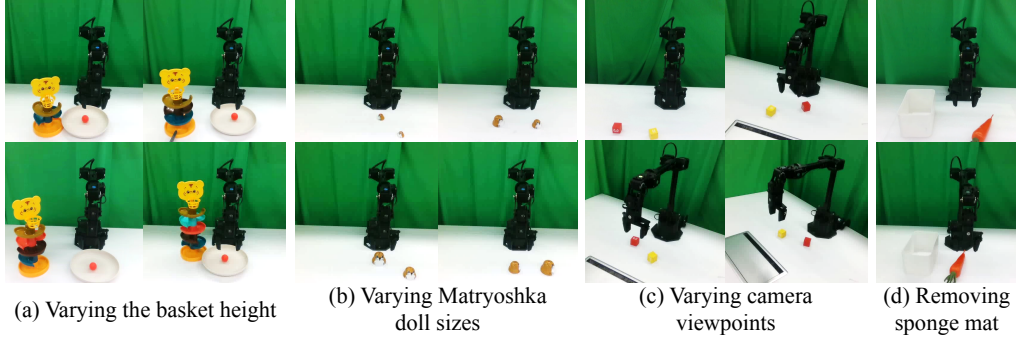


Figure 4: **Task variation visualization.** Four types of variation are conducted: (a) basket height, (b) Matryoshka doll sizes, (c) camera viewpoints, and (d) presence/absence of the sponge mat.

Table 5: **Success rate (%) under varying basket heights.** L2 and L1 indicate the basket is placed 2 and 1 layers lower than the training (Base), respectively. H1 indicates 1 layer higher.

Method	L2	L1	Base	H1
π_0 (Black et al., 2025)	50	40	50	20
CogACT (Li et al., 2024)	20	30	60	20
GeoVLA (Ours)	50	70	90	60

Table 6: **Success rate (%) under varying doll sizes.** Base refers to the training size. S1 denotes a smaller size, while L1 and L2 represent slightly and significantly larger dolls, respectively.

Method	S1	Base	L1	L2
π_0 (Black et al., 2025)	10	50	20	0
CogACT (Li et al., 2024)	70	70	40	50
GeoVLA (Ours)	70	70	80	80

5.2 Main Results

Evaluation of GeoVLA is conducted on a set of in-domain tasks, including both basic manipulation and 3D-aware tasks, with identical training and inference setups. We also compare our results against several state-of-the-art baselines, including OpenVLA (Kim et al., 2025b), π_0 (Black et al., 2025) (without pose states and other images as input), and CogACT (Li et al., 2024). As shown in Tab. 4, most models perform well on simple pick-and-place tasks, such as *Pick Carrot*, achieving a 100% success rate. However, performance drops significantly on tasks that require precise 3D spatial understanding, like *Put Basketball* and *Pick Hairclip*. In these tasks, our approach consistently outperforms others, showing better robustness and spatial awareness. Specifically, Our model achieves average success rates of 95.0% on basic tasks and 77.5% on 3D-aware tasks, yielding an overall average success rate of 86.3%, which outperforms π_0 and CogACT 28.8% and 10.0% respectively by a clear margin.

5.3 Variant Results

To further assess the robustness and generalization ability of our GeoVLA, we introduce controlled task variations that were not seen during training. As shown in Fig. 4, for each variation, a specific task setup is modified while keeping all other conditions unchanged.

Put Basketball variation Task. The training data only includes a basket positioned at the fifth layer (*Base*). During inference, the model is tested with varying basket heights at the third (*L2*), fourth (*L1*), and sixth layers (*H1*). As shown in Tab. 5, the 2D-VLA models like CogACT experience a performance drop when the basket height deviates from the training condition, achieving success rates of only 20% and 30% at *L2* and *L1*, respectively, while π_0 achieves a similar success rate compared to *Base*, struggling at picking precisely. In contrast, GeoVLA exhibits stronger generalization, keeping reasonable performance across all variations and achieving a 60% success rate even at the highest basket position (*H1*). This shows the robustness of GeoVLA to spatial distribution shifts.

Cover Matryoshka variation Task. The model is trained using a medium-sized doll (*Base*). During inference, we evaluate the model by scaling the doll to different sizes: a smaller size (*S1*), a slightly larger size (*L1*), and a significantly larger size (*L2*), to assess its robustness to scale variations. The results are summarized in Tab. 6. Compared to other 2D-VLA models, our GeoVLA consistently achieves higher success rates at larger sizes (*L1* and *L2*).

Table 7: **Success rate (%) under varying camera views.** Evaluation was conducted at 15°, 30°, and 45° viewpoints.

Method	Base	15°	30°	45°
π_0 (Black et al., 2025)	50	50	40	30
CogACT (Li et al., 2024)	80	60	40	0
GeoVLA (Ours)	90	90	80	70

Table 8: **Success rate (%) with or without the sponge mat in the Pick Carrot Task.** GeoVLA shows strong generalization.

Method	with	without
π_0 (Black et al., 2025)	100	60
CogACT (Li et al., 2024)	100	10
GeoVLA (Ours)	100	50

Stack Block variation Task. we jointly train the models using only the main camera, alongside other tasks with a side camera to enhance generalization. During inference, all the models are evaluated under specific camera views. As shown in Tab. 7, both CogACT (Li et al., 2024) and our GeoVLA perform well when the camera pose matches the training setting (*Base*). However, when the camera shifts to 45°, GeoVLA maintains high performance, while the performance of CogACT (Li et al., 2024) drops significantly.

Pick Carrot variation Task. The sponge mat present during training is removed during inference, resulting in a lower placement of the carrot. While most methods attempt to grasp the carrot from above, leading to failure, our geometric-aware GeoVLA consistently achieves more stable and successful grasps, demonstrating stronger generalization to this change.

6 Conclusion

In this paper, we investigated how to effectively integrate 3D representations into Vision-Language Action (VLA) models and proposed GeoVLA. To extract compact representations from noisy point clouds, GeoVLA employs a dual-path Point Embedding Network, which selects a token corresponding to the end-effector position as an anchor for geometric features. Coupled with vision-language features from a pre-trained VLM, a diffusion-based action head, 3D-enhanced Action Expert, processes both modalities to progressively generate action chunks. To mitigate the bias toward vision-language inputs, we further introduced multiple experts and a manually designed expert-balancing strategy. We evaluated GeoVLA in both simulation and real-world experiments, where it demonstrates strong performance. Notably, compared with 2D-VLA baselines, GeoVLA achieves significantly better results under 3D-related variations such as camera viewpoint changes, highlighting the effectiveness of integrating 3D representations into VLA models.

References

- Jean-Baptiste Alayrac, Jeff Donahue, Pauline Luc, Antoine Miech, Iain Barr, Yana Hasson, Karel Lenc, Arthur Mensch, Katie Millican, Malcolm Reynolds, Roman Ring, Eliza Rutherford, Serkan Cabi, Tengda Han, Zhitao Gong, Sina Samangooei, Marianne Monteiro, Jacob Menick, Sebastian Borgeaud, Andrew Brock, Aida Nematzadeh, Sahand Sharifzadeh, Mikolaj Binkowski, Ricardo Barreira, Oriol Vinyals, Andrew Zisserman, and Karen Simonyan. Flamingo: a visual language model for few-shot learning. In *Advances in Neural Information Processing Systems (NeurIPS)*, pages 23716–23736, 2022.
- Jinze Bai, Shuai Bai, Yunfei Chu, Zeyu Cui, Kai Dang, Xiaodong Deng, Yang Fan, Wenbin Ge, Yu Han, Fei Huang, Binyuan Hui, Luo Ji, Mei Li, Junyang Lin, Runji Lin, Dayiheng Liu, Gao Liu, Chengqiang Lu, Keming Lu, Jianxin Ma, Rui Men, Xingzhang Ren, Xuancheng Ren, Chuanqi Tan, Sinan Tan, Jianhong Tu, Peng Wang, Shijie Wang, Wei Wang, Shengguang Wu, Benfeng Xu, Jin Xu, An Yang, Hao Yang, Jian Yang, Shusheng Yang, Yang Yao, Bowen Yu, Hongyi Yuan, Zheng Yuan, Jianwei Zhang, Xingxuan Zhang, Yichang Zhang, Zhenru Zhang, Chang Zhou, Jingren Zhou, Xiaohuan Zhou, and Tianhang Zhu. Qwen technical report. *arXiv preprint arXiv:2309.16609*, 2023.
- V.S.K. Pandi V Bhat, Yu-Hsiang Lan, Prashanth Krishnamurthy, Ramesh Karri, and Farshad Khorrami. 3d cavla: Leveraging depth and 3d context to generalize vision language action models for unseen tasks. In *IEEE/CVF Conference on Computer Vision and Pattern Recognition Workshops (CVPRW)*, 2025.
- Johan Bjorck, Fernando Castañeda, Nikita Cherniadev, Xingye Da, Runyu Ding, Linxi Jim Fan, Yu Fang, Dieter Fox, Fengyuan Hu, Spencer Huang, Joel Jang, Zhenyu Jiang, Jan Kautz, Kaushil Kundalia, Lawrence Lao, Zhiqi Li, Zongyu Lin, Kevin Lin, Guilin Liu, Edith Llonet, Loic Magne, Ajay Mandlekar, Avnish Narayan, Soroush Nasiriany, Scott Reed, You Liang Tan, Guanzhi Wang, Zu Wang, Jing Wang, Qi Wang, Jiannan Xiang, Yuqi Xie, Yinzhen Xu, Zhenjia Xu, Seonghyeon Ye, Zhiding Yu, Ao Zhang, Hao Zhang, Yizhou Zhao, Ruijie Zheng, and Yuke Zhu. Gr00t n1: An open foundation model for generalist humanoid robots. *arXiv preprint arXiv:2503.14734*, 2025.

- Kevin Black, Noah Brown, Danny Driess, Adnan Esmail, Michael Equi, Chelsea Finn, Niccolo Fusai, Lachy Groom, Karol Hausman, Brian Ichter, Szymon Jakubczak, Tim Jones, Liyiming Ke, Sergey Levine, Adrian Li-Bell, Mohith Mothukuri, Suraj Nair, Karl Pertsch, Lucy Xiaoyang Shi, James Tanner, Quan Vuong, Anna Walling, Haohuan Wang, and Ury Zhilinsky. π_0 : A vision-language-action flow model for general robot control. In *Robotics: Science and Systems (RSS)*, 2025.
- Anthony Brohan, Noah Brown, Justice Carbajal, Yevgen Chebotar, Xi Chen, Krzysztof Choromanski, Tianli Ding, Danny Driess, Avinava Dubey, Chelsea Finn, Pete Florence, Chuyuan Fu, Montse Gonzalez Arenas, Keerthana Gopalakrishnan, Kehang Han, Karol Hausman, Alexander Herzog, Jasmine Hsu, Brian Ichter, Alex Irpan, Nikhil Joshi, Ryan Julian, Dmitry Kalashnikov, Yuheng Kuang, Isabel Leal, Lisa Lee, Tsang-Wei Edward Lee, Sergey Levine, Yao Lu, Henryk Michalewski, Igor Mordatch, Karl Pertsch, Kanishka Rao, Krista Reymann, Michael Ryoo, Grecia Salazar, Pannag Sanketi, Pierre Sermanet, Jaspiar Singh, Anikait Singh, Radu Soricut, Huong Tran, Vincent Vanhoucke, Quan Vuong, Ayzaan Wahid, Stefan Welker, Paul Wohlhart, Jialin Wu, Fei Xia, Ted Xiao, Peng Xu, Sichun Xu, Tianhe Yu, and Brianna Zitkovich. Rt-2: Vision-language-action models transfer web knowledge to robotic control. In *The Conference on Robot Learning (CoRL)*, pages 2165–2183, 2023a.
- Anthony Brohan, Noah Brown, Justice Carbajal, Yevgen Chebotar, Joseph Dabis, Chelsea Finn, Keerthana Gopalakrishnan, Karol Hausman, Alex Herzog, Jasmine Hsu, Julian Ibarz, Brian Ichter, Alex Irpan, Tomas Jackson, Sally Jesmonth, Nikhil J Joshi, Ryan Julian, Dmitry Kalashnikov, Yuheng Kuang, Isabel Leal, Kuang-Huei Lee, Sergey Levine, Yao Lu, Utsav Malla, Deeksha Manjunath, Igor Mordatch, Ofir Nachum, Carolina Parada, Jodilyn Peralta, Emily Perez, Karl Pertsch, Jornell Quiambao, Kanishka Rao, Michael Ryoo, Grecia Salazar, Pannag Sanketi, Kevin Sayed, Jaspiar Singh, Sumedh Sontakke, Austin Stone, Clayton Tan, Huong Tran, Vincent Vanhoucke, Steve Vega, Quan Vuong, Fei Xia, Ted Xiao, Peng Xu, Sichun Xu, Tianhe Yu, and Brianna Zitkovich. Rt-1: Robotics transformer for real-world control at scale. In *Robotics: Science and Systems (RSS)*, 2023b.
- Xi Chen, Xiao Wang, Soravit Changpinyo, AJ Piergiovanni, Piotr Padlewski, Daniel Salz, Sebastian Goodman, Adam Grycner, Basil Mustafa, Lucas Beyer, Alexander Kolesnikov, Joan Puigcerver, Nan Ding, Keran Rong, Hassan Akbari, Gaurav Mishra, Linting Xue, Ashish Thapliyal, James Bradbury, Weicheng Kuo, Mojtaba Seyedhosseini, Chao Jia, Burcu Karagol Ayan, Carlos Riquelme, Andreas Steiner, Anelia Angelova, Xiaohua Zhai, Neil Houlsby, and Radu Soricut. PaLI: A jointly-scaled multilingual language-image model. In *International Conference on Learning Representations (ICLR)*, 2023.
- Runpei Dong, Zekun Qi, Linfeng Zhang, Junbo Zhang, Jianjian Sun, Zheng Ge, Li Yi, and Kaisheng Ma. Autoencoders as cross-modal teachers: Can pretrained 2d image transformers help 3d representation learning? In *International Conference on Learning Representations (ICLR)*, 2023.
- Ankit Goyal, Valts Blukis, Jie Xu, Yijie Guo, Yu-Wei Chao, and Dieter Fox. Rvt-2: Learning precise manipulation from few demonstrations. In *Robotics: Science and Systems Workshop (RSSW)*, 2024.
- Jonathan Ho, Ajay Jain, and Pieter Abbeel. Denoising diffusion probabilistic models. In *Advances in Neural Information Processing Systems (NeurIPS)*, pages 6840–6851, 2020.
- Zhi Hou, Tianyi Zhang, Yuwen Xiong, Haonan Duan, Hengjun Pu, Ronglei Tong, Chengyang Zhao, Xizhou Zhu, Yu Qiao, Jifeng Dai, and Yuntao Chen. Dita: Scaling diffusion transformer for generalist vision-language-action policy. *arXiv preprint arXiv:2503.19757*, 2025.
- Yueru Jia, Jiaming Liu, Sixiang Chen, Chenyang Gu, Zhilue Wang, Longzan Luo, Lily Lee, Pengwei Wang, Zhongyuan Wang, Renrui Zhang, and Shanghang Zhang. Lift3d foundation policy: Lifting 2d large-scale pretrained models for robust 3d robotic manipulation. *arXiv preprint arXiv:2411.18623*, 2024.
- Siddharth Karamcheti, Suraj Nair, Ashwin Balakrishna, Percy Liang, Thomas Kollar, and Dorsa Sadigh. Prismatic vlms: Investigating the design space of visually-conditioned language models. In *International Conference on Machine Learning (ICML)*, 2024.
- Moo Jin Kim, Chelsea Finn, and Percy Liang. Fine-tuning vision-language-action models: Optimizing speed and success. In *Robotics: Science and Systems (RSS)*, 2025a.
- Moo Jin Kim, Karl Pertsch, Siddharth Karamcheti, Ted Xiao, Ashwin Balakrishna, Suraj Nair, Rafael Rafailov, Ethan Foster, Grace Lam, Pannag Sanketi, Quan Vuong, Thomas Kollar, Benjamin Burchfiel, Russ Tedrake, Dorsa Sadigh, Sergey Levine, Percy Liang, and Chelsea Finn. Openvla: An open-source vision-language-action model. In *The Conference on Robot Learning (CoRL)*, 2025b.
- Chengmeng Li, Junjie Wen, Yan Peng, Yaxin Peng, Feifei Feng, and Yichen Zhu. Pointvla: Injecting the 3d world into vision-language-action models. *arXiv preprint arXiv:2503.07511*, 2025.

- Qixiu Li, Yaobo Liang, Zeyu Wang, Lin Luo, Xi Chen, Mozheng Liao, Fangyun Wei, Yu Deng, Sicheng Xu, Yizhong Zhang, Xiaofan Wang, Bei Liu, Jianlong Fu, Jianmin Bao, Dong Chen, Yuanchun Shi, Jiaolong Yang, and Baining Guo. Cogact: A foundational vision-language-action model for synergizing cognition and action in robotic manipulation. *arXiv preprint arXiv:2411.19650*, 2024.
- Yaron Lipman, Ricky TQ Chen, Heli Ben-Hamu, Maximilian Nickel, and Matt Le. Flow matching for generative modeling. *arXiv preprint arXiv:2210.02747*, 2022.
- Bo Liu, Yifeng Zhu, Chongkai Gao, Yihao Feng, Qiang Liu, Yuke Zhu, and Peter Stone. Libero: Benchmarking knowledge transfer for lifelong robot learning. In *Advances in Neural Information Processing Systems (NeurIPS)*, pages 44776–44791, 2023a.
- Haotian Liu, Chunyuan Li, Qingyang Wu, and Yong Jae Lee. Visual instruction tuning. In *Advances in Neural Information Processing Systems (NeurIPS)*, pages 34892–34916, 2023b.
- Jiaming Liu, Hao Chen, Pengju An, Zhuoyang Liu, Renrui Zhang, Chenyang Gu, Xiaoqi Li, Ziyu Guo, Sixiang Chen, Mengzhen Liu, Chengkai Hou, Mengdi Zhao, KC alex Zhou, Pheng-Ann Heng, and Shanghang Zhang. Hybridvla: Collaborative diffusion and autoregression in a unified vision-language-action model. *arXiv preprint arXiv:2503.10631*, 2025a.
- Songming Liu, Lingxuan Wu, Bangguo Li, Hengkai Tan, Huayu Chen, Zhengyi Wang, Ke Xu, Hang Su, and Jun Zhu. Rdt-1b: a diffusion foundation model for bimanual manipulation. In *International Conference on Learning Representations (ICLR)*, 2025b.
- Ilya Loshchilov and Frank Hutter. Decoupled weight decay regularization. In *International Conference on Learning Representations (ICLR)*, 2019.
- Paulius Micikevicius, Sharan Narang, Jonah Alben, Gregory Diamos, Erich Elsen, David Garcia, Boris Ginsburg, Michael Houston, Oleksii Kuchaiev, Ganesh Venkatesh, and Hao Wu. Mixed precision training. In *International Conference on Learning Representations (ICLR)*, 2018.
- Tongzhou Mu, Zhan Ling, Fanbo Xiang, Derek Yang, Xuanlin Li, Stone Tao, Zhiao Huang, Zhiwei Jia, and Hao Su. Maniskill: Generalizable manipulation skill benchmark with large-scale demonstrations. In *Advances in Neural Information Processing Systems (NeurIPS)*, 2021.
- Dantong Niu, Yuvan Sharma, Giscard Biamby, Jerome Quenum, Yutong Bai, Baifeng Shi, Trevor Darrell, and Roei Herzig. Llarva: Vision-action instruction tuning enhances robot learning. In *The Conference on Robot Learning (CoRL)*, 2024.
- Octo Model Team, Dibya Ghosh, Homer Walke, Karl Pertsch, Kevin Black, Oier Mees, Sudeep Dasari, Joey Hejna, Charles Xu, Jianlan Luo, Tobias Kreiman, You Liang Tan, Lawrence Yunliang Chen, Pannag Sanketi, Quan Vuong, Ted Xiao, Dorsa Sadigh, Chelsea Finn, and Sergey Levine. Octo: An open-source generalist robot policy. In *Robotics: Science and Systems (RSS)*, 2024.
- Abby O’Neill, Abdul Rehman, Abhiram Maddukuri, Abhishek Gupta, Abhishek Padalkar, Abraham Lee, Acorn Pooley, Agrim Gupta, Ajay Mandlekar, Ajinkya Jain, et al. Open x-embodiment: Robotic learning datasets and rt-x models: Open x-embodiment collaboration 0. In *IEEE International Conference on Robotics and Automation (ICRA)*, pages 6892–6903, 2024.
- William Peebles and Saining Xie. Scalable diffusion models with transformers. In *IEEE/CVF International Conference on Computer Vision (ICCV)*, pages 4195–4205, 2023.
- Karl Pertsch, Kyle Stachowicz, Brian Ichter, Danny Driess, Suraj Nair, Quan Vuong, Oier Mees, Chelsea Finn, and Sergey Levine. Fast: Efficient action tokenization for vision-language-action models. In *Robotics: Science and Systems (RSS)*, 2025.
- Charles R Qi, Hao Su, Kaichun Mo, and Leonidas J. Guibas. Pointnet: Deep learning on point sets for 3d classification and segmentation. In *IEEE Conference on Computer Vision and Pattern Recognition (CVPR)*, pages 652–660, 2017.
- Delin Qu, Haoming Song, Qizhi Chen, Yuanqi Yao, Xinyi Ye, Yan Ding, Zhigang Wang, JiaYuan Gu, Bin Zhao, Dong Wang, and Xuelong Li. Spatialvla: Exploring spatial representations for visual-language-action model. In *Robotics: Science and Systems (RSS)*, 2025.
- Mohit Shridhar, Lucas Manuelli, and Dieter Fox. Perceiver-actor: A multi-task transformer for robotic manipulation. In *Conference on Robot Learning*, pages 785–799, 2023.
- Jiaming Song, Chenlin Meng, and Stefano Ermon. Denoising diffusion implicit models. In *International Conference on Learning Representations (ICLR)*, 2021.

- Jianlin Su, Murtadha Ahmed, Yu Lu, Shengfeng Pan, Wen Bo, and Yunfeng Liu. Roformer: Enhanced transformer with rotary position embedding. *Neurocomputing*, 568:127063, 2024.
- Tai Wang, Xiaohan Mao, Chenming Zhu, Runsen Xu, Ruiyuan Lyu, Peisen Li, Xiao Chen, Wenwei Zhang, Kai Chen, Tianfan Xue, Xihui Liu, Cewu Lu, Dahua Lin, and Jiangmiao Pang. Embodiedscan: A holistic multi-modal 3d perception suite towards embodied ai. In *IEEE/CVF Conference on Computer Vision and Pattern Recognition*, pages 19757–19767, 2024.
- Yu Xiang, Tanner Schmidt, Venkatraman Narayanan, and Dieter Fox. Posecnn: A convolutional neural network for 6d object pose estimation in cluttered scenes. In *Robotics: Science and Systems (RSS)*, 2018.
- Yanjie Ze, Gu Zhang, Kangning Zhang, Chenyuan Hu, Muhan Wang, and Huazhe Xu. 3d diffusion policy: Generalizable visuomotor policy learning via simple 3d representations. In *Robotics: Science and Systems (RSS)*, 2024.
- Lvmin Zhang, Anyi Rao, and Maneesh Agrawala. Adding conditional control to text-to-image diffusion models. In *IEEE/CVF International Conference on Computer Vision (ICCV)*, pages 3813–3824, 2023.
- Yani Zhang, Dongming Wu, Hao Shi, Yingfei Liu, Tiancai Wang, Haoqiang Fan, and Xingping Dong. Grounding beyond detection: Enhancing contextual understanding in embodied 3d grounding. *arXiv preprint arXiv:2506.05199*, 2025.
- Tony Z Zhao, Vikash Kumar, Sergey Levine, and Chelsea Finn. Learning fine-grained bimanual manipulation with low-cost hardware. In *Robotics: Science and Systems (RSS)*, 2023.
- Haoyu Zhen, Xiaowen Qiu, Peihao Chen, Jincheng Yang, Xin Yan, Yilun Du, Yining Hong, and Chuang Gan. 3d-vla: A 3d vision-language-action generative world model. *arXiv preprint arXiv:2403.09631*, 2024a.
- Haoyu Zhen, Xiaowen Qiu, Peihao Chen, Jincheng Yang, Xin Yan, Yilun Du, Yining Hong, and Chuang Gan. 3d-vla: A 3d vision-language-action generative world model. In *International Conference on Machine Learning (ICML)*, pages 61229–61245, 2024b.
- Henry Zheng, Hao Shi, Qihang Peng, Yong Xien Chng, Rui Huang, Yepeng Weng, Zhongchao Shi, and Gao Huang. Densegrounding: Improving dense language-vision semantics for ego-centric 3d visual grounding. *arXiv preprint arXiv:2505.04965*, 2025.
- Chenming Zhu, Tai Wang, Wenwei Zhang, Jiangmiao Pang, and Xihui Liu. Llava-3d: A simple yet effective pathway to empowering lmms with 3d-awareness. *arXiv preprint arXiv:2409.18125*, 2024.

A Simulation Environments

Fig. 5 gives the overall visualization of the two simulation benchmarks including LIBERO and ManiSkill2 in our experiments. The LIBERO benchmark consists of five task suites focusing on different skills, while the ManiSkill2 benchmarks focus primarily on pick-and-place scenarios.

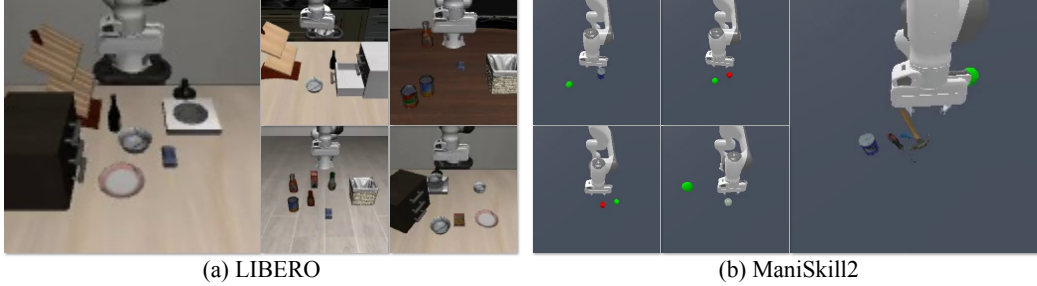


Figure 5: **Simulation benchmarks.** The LIBERO benchmark (a) contains various scenes and tasks, and the ManiSkill2 benchmark Pick-and-Place tasks (b) are required to pick an object to the specific location marked by a green point in a 3D space.

B Visualization of Simulation Results

Fig. 6 and Fig. 7 present qualitative results on representative tasks from LIBERO and ManiSkill2, respectively. These visualizations demonstrate that our approach can accurately recognize and interact with the objects in different tasks and different environments, highlighting its strong performance and adaptability.

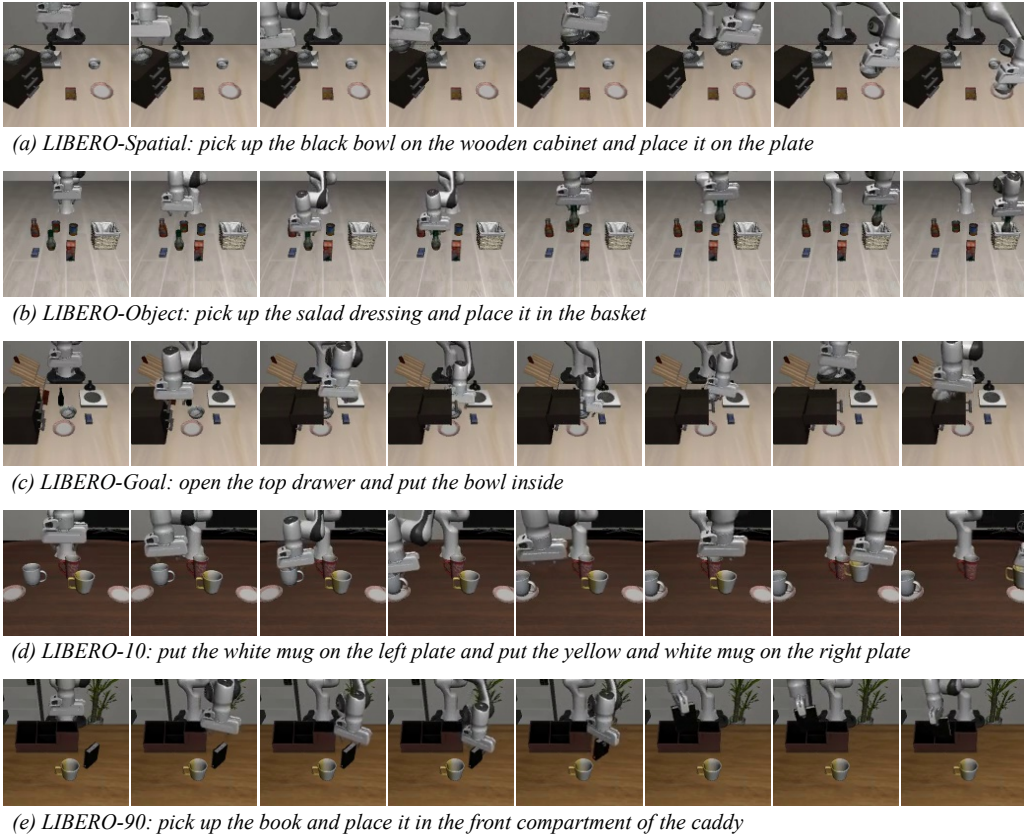


Figure 6: **Qualitative results of GeoVLA** on the five task suites of LIBERO benchmark.

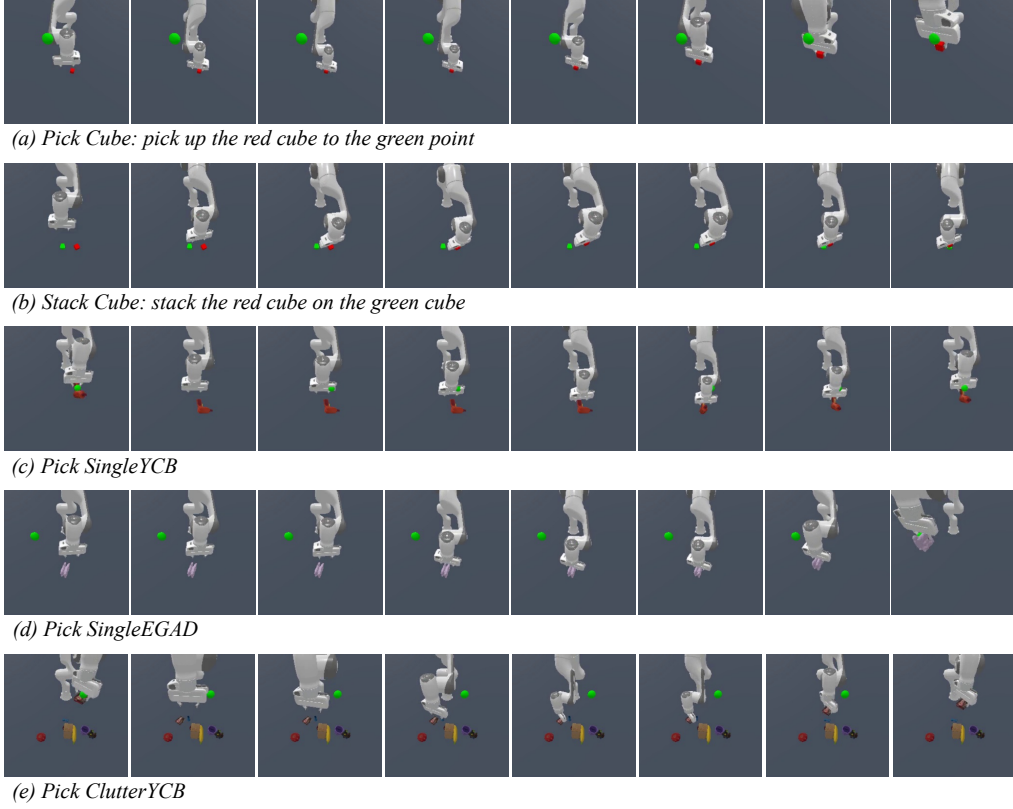


Figure 7: **Qualitative results of GeoVLA** on the five tasks of ManiSkill2 benchmark.

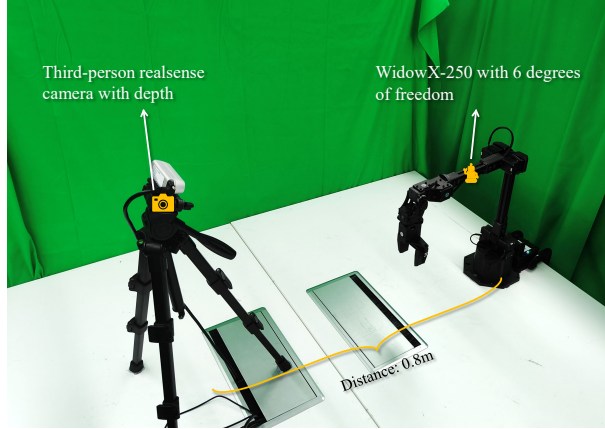


Figure 8: **Setup of real experiments.** We describe our real-world experimental setup, which includes a depth camera and a robotic arm.

C Real-World Environments

In our real-world experiments, we employ a WidowX-250s robotic arm with six degrees of freedom and a RealSense-435i depth camera placed approximately 0.8 meters away to capture a third-person viewpoint, as shown in Fig. 8. The basic tasks and 3D-aware tasks we conduct in our real-world experiments are shown below and the overall visualization is shown in Fig. 9.

Base Tasks. We consider four fundamental manipulation tasks designed to evaluate basic pick-and-place capabilities: (1) *Pick Carrot*: The robot is required to grasp a slender carrot and place it into a

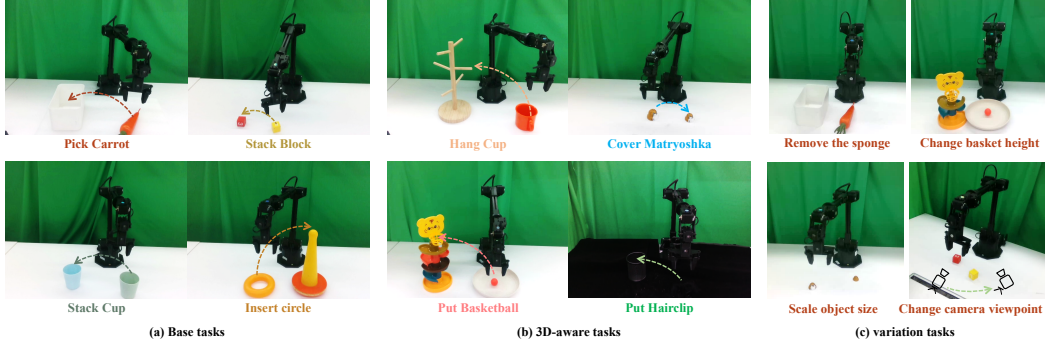


Figure 9: **Tasks in real-world experiments.** We divide the tasks into two categories: (a) base tasks designed to evaluate essential pick-and-place abilities; (b) 3D-aware tasks that require more accurate spatial reasoning and object pose estimation; and (c) task variations used at inference time to assess robustness and generalization.

box; (2) *Stack Block* and (3) *Stack Cup*: The robot needs to pick up a yellow block or a green cup and stack it onto another object; (4) *Insert Circle*: The robot must pick up a circular object and insert it into a vertical pillar. These base tasks are jointly trained to improve training efficiency and facilitate shared skill learning.

3D-Aware Tasks. We also design a set of more challenging tasks that require accurate perception of object poses and spatial relationships in 3D space: (1) *Hang Cup*: The robot must grasp a cup and precisely hang it on a narrow holder; (2) *Put Basketball*: The robot picks up a basketball and places it into a basket; (3) *Cover Matryoshka*: The robot needs to pick up a larger Matryoshka doll and cover a smaller one; (4) *Put Hairclip*: The robot is required to pick up a **black** hairclip and place it into a bucket located inside a **black** desk—this presents significant challenges for RGB-based perception due to low color contrast and background ambiguity. Unlike the base tasks, each 3D-aware task is trained independently to avoid task interference, ensuring that generalization capabilities are learned from the model architecture and spatial understanding.

D Visualization of Real-World Results

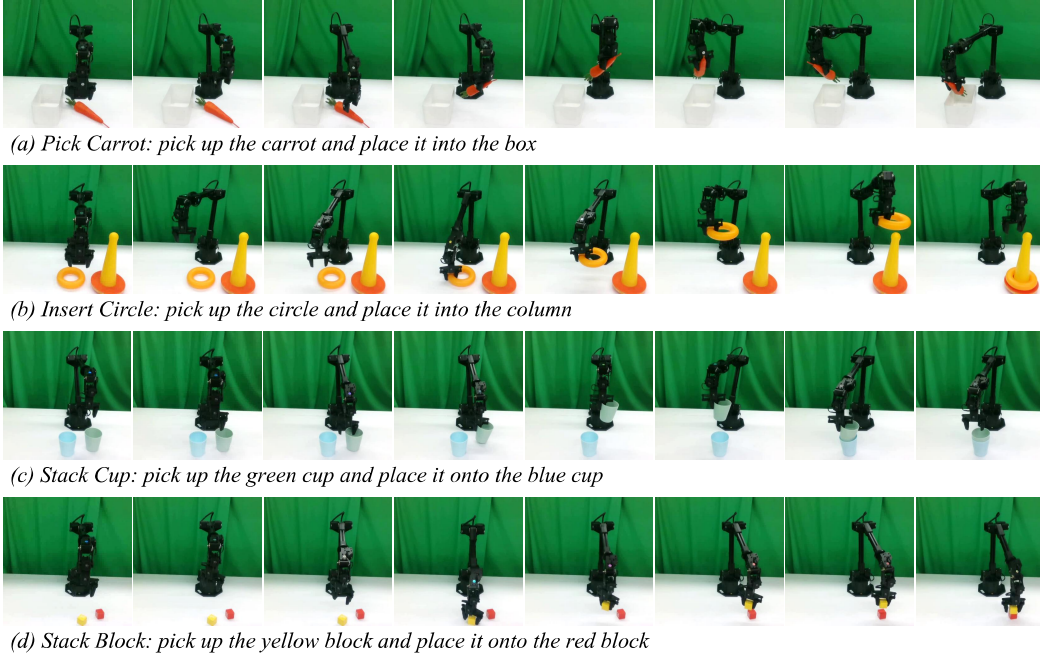


Figure 10: **Examples of base task executions with GeoVLA.**

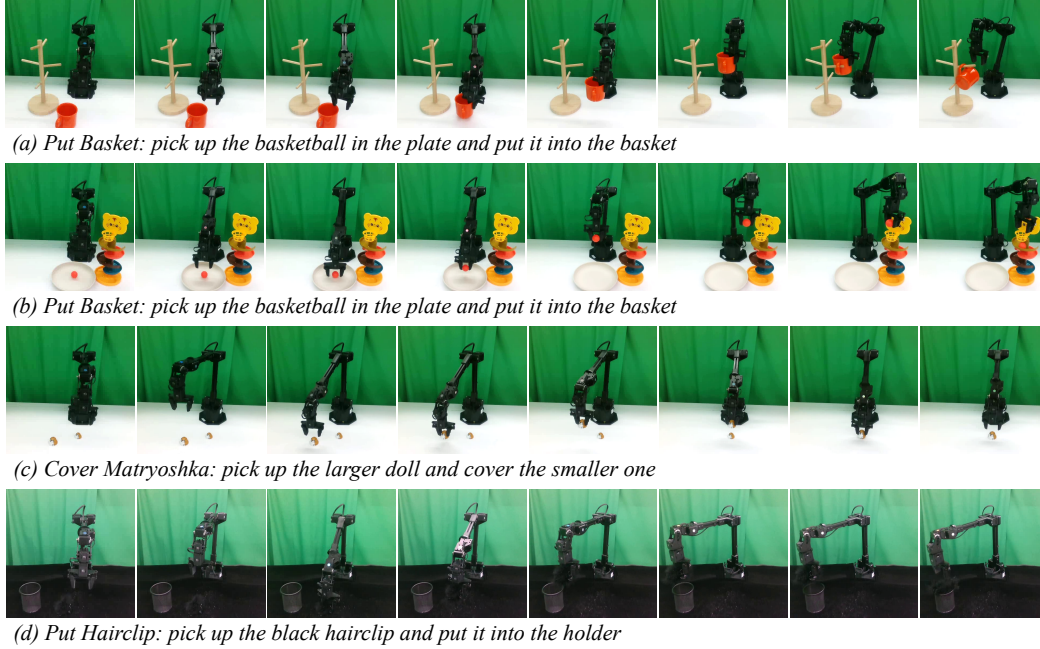


Figure 11: Examples of 3D-aware task executions with GeoVLA.

Fig. 10 and Fig. 11 illustrate the qualitative performance of GeoVLA on base tasks and 3D-aware tasks, respectively. GeoVLA demonstrates high precision and success rates across all tasks. In particular, for 3D-aware tasks such as the *Put Hairclip* task, GeoVLA effectively leverages point cloud inputs to extract detailed geometric structures, enabling robust performance even in the absence of RGB inputs.

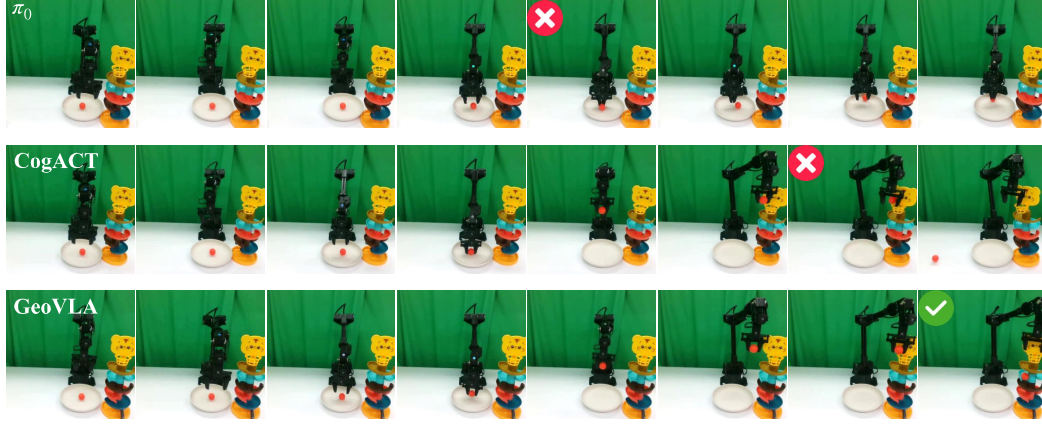
In addition, Fig. 12 demonstrates that our proposed GeoVLA outperforms other SoTA methods such as π_0 (Black et al. (2025)) and CogACT (Li et al. (2024)) by accurately recognizing the 3D positions in the *Put Basketball* variation tasks. Fig. 13 shows that GeoVLA maintains strong performance when scaling the size of the dolls. Fig. 14 further illustrates the robustness of GeoVLA to camera viewpoint changes.

E More Experiments on Generalization

To evaluate the robustness of the GeoVLA to the background and lightness, we conduct the experiments of changing the background and lightness on some basic tasks as shown in Tab. 9. Fig. 15 also shows some qualitative visualizations.

Table 9: **Success rate (%) under background and lighting variations** on three distinct manipulation tasks.

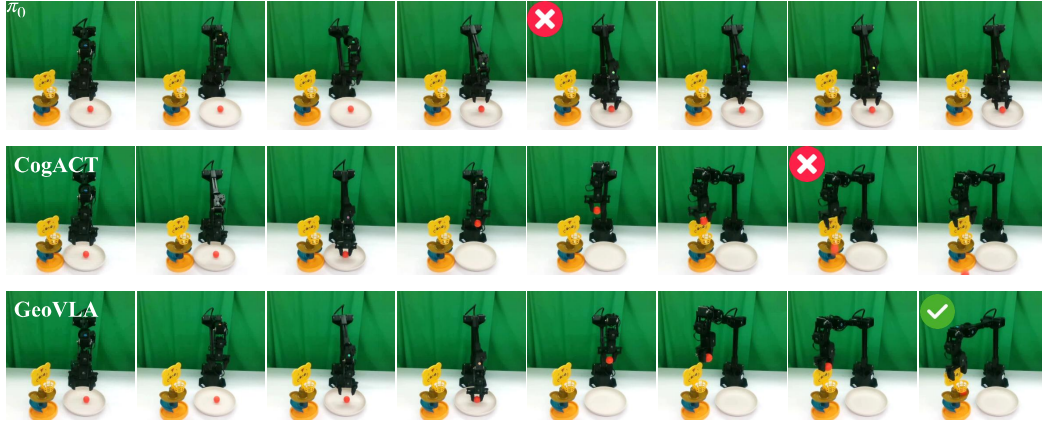
Setting	Stack Cup	Insert Circle	Stack Block	Avg.
w/o background change	100	100	80	93.3
w/ background change	90	70	80	80.0
w/ light change	100	70	50	73.3



(a) Put Basketball Variation: **one layer higher** than the training.

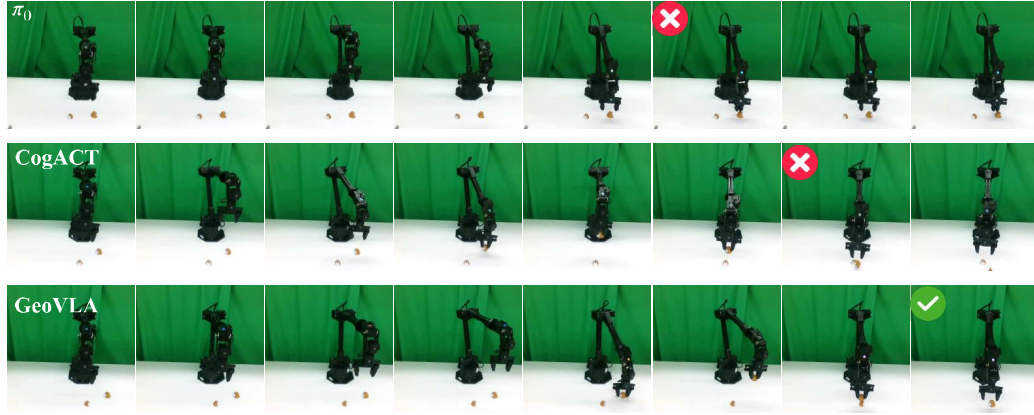


(b) Put Basketball Variation: **one layer lower** than the training.

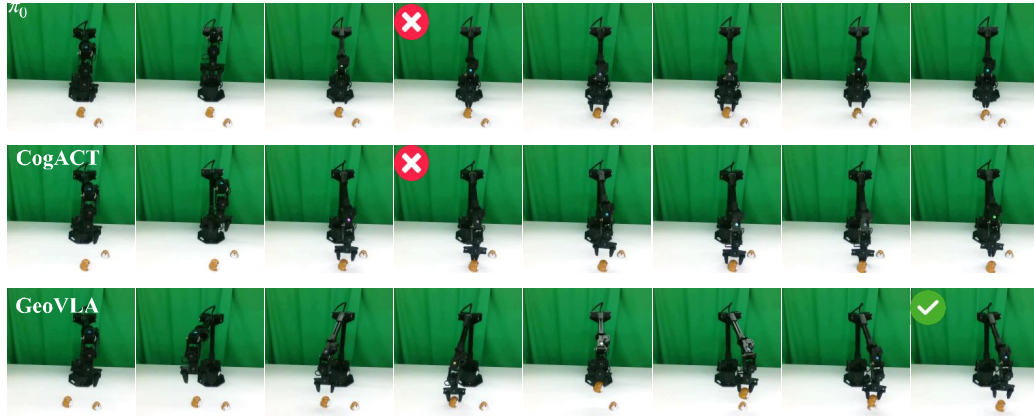


(c) Put Basketball Variation: **two layer lower** than the training.

Figure 12: **Qualitative comparison with π_0 and CogACT** on the *Put Basketball* variation tasks. GeoVLA performs well on both higher and lower basketball position.



(a) Cover Matryashka Variation: **smaller** than the training.

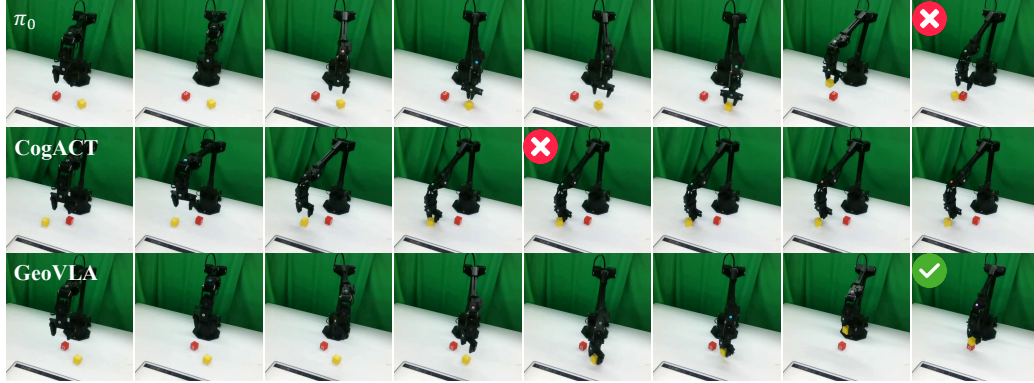


(b) Cover Matryashka Variation: **larger** than the training.

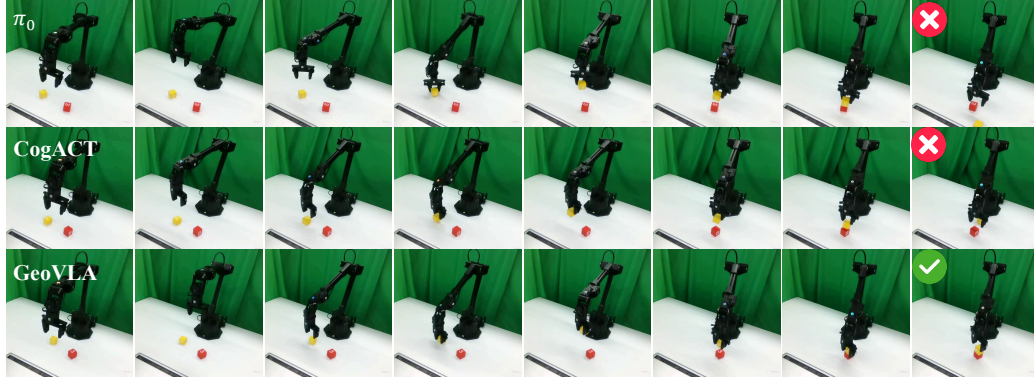


(c) Cover Matryashka Variation: **much larger** than the training.

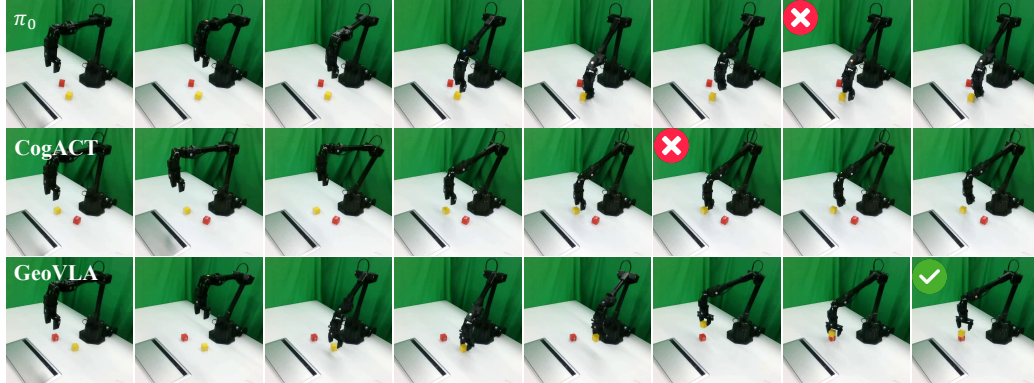
Figure 13: **Qualitative comparison with π_0 and CogACT** on the *Cover Matryashka* variation tasks. GeoVLA performs well on both larger and smaller doll sizes.



(a) Stack Block Variation: a 15-degree shift compared to the training setting



(b) Stack Block Variation: a 30-degree shift compared to the training setting

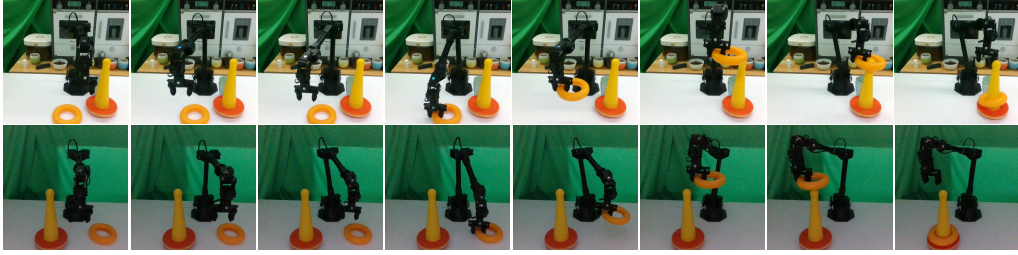


(c) Stack Block Variation: a 45-degree shift compared to the training setting

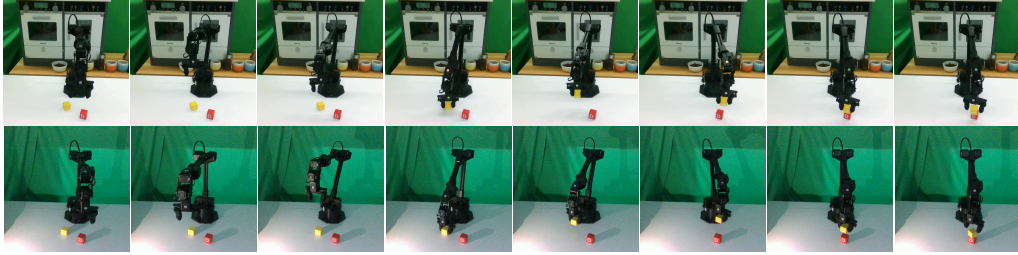
Figure 14: **Qualitative comparison with π_0 and CogACT** on the *Stack Block* variation tasks. GeoVLA performs better when the camera viewpoint changes.



(a) *Stack Cup: pick up the green cup and place it onto the blue cup*



(b) *Insert Circle: pick up the circle and place it into the column*



(c) *Stack Block: pick up the yellow block and place it onto the red block*

Figure 15: **Visualization of GeoVLA on background and light change** on the *Stack Cup*, *Insert Circle*, *Stack Block*. GeoVLA shows robustness to the background and light change.